C. R. Geoscience 350 (2018) 154–163

Contents lists available at ScienceDirect

Comptes Rendus Geoscience

www.sciencedirect.com

Petrology, Geochemistry

Salinity of the Archaean oceans from analysis of fluid inclusions in quartz

Bernard Marty [a,*], Guillaume Avice [b], David V. Bekaert [a], Michael W. Broadley [a]

[a] Centre de recherches pétrographiques et géochimiques, CNRS, Université de Lorraine, 15, rue Notre-Dame-des-Pauvres, 54500 Vandœuvre-lès-Nancy, France

[b] California Institute of Technology, Division of Geological and Planetary Sciences, 1200 E. California Blvd, Pasadena, CA 91125, USA

ARTICLE INFO

Article history:
Received 27 November 2017
Accepted after revision 12 December 2017
Available online 2 April 2018

Handled by Marc Chaussidon

Keywords:
Salinity
Archean oceans
Noble gases

ABSTRACT

Fluids trapped in inclusions in well-characterized Archaean hydrothermal quartz crystals were analyzed by the extended argon–argon method, which permits the simultaneous measurement of chlorine and potassium concentrations. Argon and nitrogen isotopic compositions of the trapped fluids were also determined by static mass spectrometry. Fluids were extracted by stepwise crushing of quartz samples from North Pole (NW Australia) and Barberton (South Africa) 3.5–3.0-Ga-old greenstone belts. The data indicate that fluids are a mixture of a low salinity end-member, regarded as the Archaean oceanic water, and several hydrothermal end-members rich in Cl, K, N, and radiogenic parentless ^{40}Ar. The low Cl–K end-member suggests that the salinity of the Archaean oceans was comparable to the modern one, and that the potassium content of the Archaean oceans was lower than at present by about 40%. A constant salinity of the oceans through time has important implications for the stabilization of the continental crust and for the habitability of the ancient Earth.

1. Introduction

Prokaryotic microbial life was already present during the Archaean aeon 3.8–2.5 Ga ago (Knauth, 2005, and refs. therein). These ancient forms of life developed in the Archaean oceans, whose properties – salinity, temperature, chemistry – are not well understood, and are subject to debated studies. Here we focus on the salinity of the Archaean oceans. The halogens would have been delivered early to the surface of the Earth by impacting bodies as well as by catastrophic degassing of the mantle. Holland (1984) estimated that the salinity of the ancient oceans could have been ~1.2 times the modern inventory by assuming that all evaporites found on the continents were once dissolved in the oceans. Unfortunately, the extent of Precambrian evaporites is unknown, due to their poor preservation. Knauth (2005) went a step further by also considering brines in stratified oceans and those presumably preserved in continents, and proposed an Archaean ocean salinity about 1.2–2 times the modern one. These authors considered that the only efficient process to decrease the salinity of the oceans is evaporite formation and isolation onto continental platforms. Consequently, most of halogens would have remained dissolved in the oceans before the major pulses of continental growth. However, another potential pathway for halogens to escape the surface reservoirs is subduction and recycling into the mantle, as suggested by recent budgets at arcs (Kendrick et al., 2012, 2017). The flux of halogens from the mantle to the oceans and from the oceans to the oceanic crust are

* Corresponding author.
E-mail address: bernard.marty@univ-lorraine.fr (B. Marty).

https://doi.org/10.1016/j.crte.2017.12.002

also poorly constrained (Berner and Berner, 2012), and it is difficult to evaluate the salinity of ancient oceans from geochemical mass balance considerations.

The composition of fluid inclusions in selected retentive mineral phases of Archaean age have already been used to provide an insight into the composition of the past hydrosphere (de Ronde et al., 1997; Weiershauser and Spooner, 2005). This approach is not without problems, since (i) fluid inclusions are not necessarily contemporaneous with their host mineral, many of them being secondary, and (ii) trapped fluids are generally a mixture of several components including hydrothermal end-members. de Ronde et al. (1997) estimated that the Archaean oceans' salinity was about twice the modern one, from correlations between relevant chemical species in fluid inclusions trapped in quartz-goethite deposits. These samples, initially interpreted as hydrothermal chimneys older than 3.2 Ga, were later on regarded as Cenozoic spring deposits (Lowe and Byerly, 2003). From statistical analysis of fluid inclusions trapped in hydrothermal quartz in Archaean terrains worldwide, Weiershauser and Spooner (2005) suggested that the Archaean oceans could have been more saline than the present-day oceans by up to one order of magnitude.

Given their chemical inertness, noble gases behave as physical tracers in the environment. In particular, the atmospheric partial pressures of non-radiogenic argon isotopes (^{36}Ar and ^{38}Ar) are unlikely to have drastically varied in the past since the Earth's building episodes, ~4.5 Ga ago. The excellent match between the atmospheric ^{38}Ar/^{36}Ar ratio (two Ar isotopes of primordial origin) and that of Ar trapped in primitive meteorites attests that atmospheric Ar was not quantitatively lost to space. Independently, noble gas isotope systematics indicates that mantle degassing did not contribute quantitatively to the atmospheric inventory of these elements after the Earth's formation. The large difference in the ^{40}Ar/^{36}Ar values between the mantle (~10^4) and the atmosphere (298.6) implies that less than 2% of mantle ^{36}Ar has been transferred to the atmosphere since the time of the Earth's formation (e.g., Ozima and Podosek, 2002). A similar conclusion is obtained from ^{36}Ar flux estimates. The modern flux of ^{36}Ar from the mantle is ~2000 mol/year (e.g., Pujol et al., 2013 and refs. therein). Integrated over 3.5 Gy and assuming a constant flux through time, the amount of ^{36}Ar degassed from the mantle is only about 0.1% of its atmospheric inventory ($5.55 \cdot 10^{15}$ mol). The degassing rate of the mantle was probably higher in the past because of a higher thermal regime. Coltice et al. (2009) estimated that the melting rate of the mantle was by a factor of ~20 higher 3.5 Gy ago as compared to the present-day rate. In this case, the contribution of mantle ^{36}Ar degassed to the atmosphere represents only 0.8% of the ^{36}Ar inventory, which is still negligible in the context of this study. Further constraints on the behaviour of atmospheric noble gases through time stem from the analysis of paleo-atmospheric gases trapped in Archaean fluid inclusions (FIs). The isotope compositions of neon, argon (^{38}Ar/^{36}Ar) and krypton of the Archaean atmosphere were found similar to those of modern air (Avice et al., 2017; Pujol et al., 2011), suggesting (i) no, or limited, escape to space for these elements since that aeon, and (ii) weak contribution from mantle noble gases (e.g., Ne). A closed system atmosphere for inert gases, including N_2, is consistent with models of atmospheric evolution through time since the Archaean aeon (Lichtenegger et al., 2010).

The concentration of noble gases in surface water is a function of their atmospheric partial pressure (assumed to be constant for, e.g., ^{36}Ar, see above) as well as water temperature and salinity. Thus, other dissolved species of interest can be scaled to noble gas concentrations to investigate their origin and behaviour through time. Our group previously analyzed N_2 together with Ar isotopes in a suite of Archaean FI-bearing quartz. In hydrothermal quartz FIs, argon is a mixture of dissolved atmospheric Ar and of one or several hydrothermal end-members rich in radiogenic ^{40}Ar (hereby ^{40}Ar*), thus permitting the identification of mixing trends and therefore the compositions of the different components. Such identification has otherwise been a major problem in previous FI studies. Based on ^{40}Ar/^{36}Ar versus N_2/^{36}Ar correlations, Marty et al. (2013) proposed that the Archaean partial pressure of atmospheric N_2 was comparable to, or lower than, the present-day one and that the ^{15}N/^{14}N ratio did not vary significantly since 3.5 Ga ago, in agreement with results from aeronomic modelling (Lichtenegger et al., 2010). In this work, we adopt the same approach for halogens (here Cl) and potassium, also quantified together with argon isotopes in neutron-irradiated quartz (e.g., Kendrick, 2012; Kendrick et al., 2001). Using samples for which fluids trapped in FIs have been demonstrated to be Archaean (Avice et al., 2017; Marty et al., 2013; Pujol et al., 2011, 2013), we define the surface water component, presumably seawater for the Cl/^{36}Ar and K/^{36}Ar ratios, and infer its salinity from solubility data for argon.

2. Samples

Several of the present samples have been previously analyzed to get insight into the composition of the Archaean atmosphere.

2.1. Dresser formation, North Pole, Pilbara Craton, NW Australia

Samples PI-02-39-# are from the 3.49-Ga-old Dresser formation, Warrawoona Group, Pilbara Craton at North Pole (Western Australia) (Foriel et al., 2004). These are quartz-carbonate aggregates forming pods in undeformed pillow basalts at the top of the Dresser formation. Quartz contains abundant, 1–25-μm, two-phase (liquid and ~5% vapour) aqueous inclusions. They are randomly distributed throughout the host quartz, which supports a primary origin. The trapped fluids are interpreted as representing mixing between a "North Pole seawater" end-member and several hydrothermal components with variable Cl/K, Ba and metal contents. The salinity of trapped fluids is highly variable (average: ~12%) with end-member values comparable to, or lower than, that of modern seawater (Foriel et al., 2004). The age of trapped fluids is likely >2.7 Ga, and probably contemporaneous with the Dresser formation (Pujol et al., 2013). Trapped fluids contain Archaean paleo-

atmospheric argon ($^{40}Ar/^{36}Ar = 143 \pm 24$, 1σ) and xenon (Pujol et al., 2013).

Sample PI-06 consists of quartz filling 2–10 mm amygdules in komatiitic basalt from a drillcore at the base of the Dresser formation (Pujol et al., 2011). This formation never experienced a metamorphic grade higher than that of the prehnite-pumpellyite facies (Foriel et al., 2004). The Ar–Ar plateau age of that sample is by 3.0 ± 0.2 Ga, lower than the Dresser formation age, suggesting a resetting event of the Ar–Ar chronometer at that time (Pujol et al., 2011). The trapped neon and krypton have isotopic compositions similar to those of air, and xenon is mass-dependently fractionated by 1%/u, a feature typical of Archaean atmospheric Xe (Avice et al., 2017; Pujol et al., 2011).

2.2. Barberton Greenstone Belt (BGB), South Africa

BMGA-# samples are from a core drilled in the Kromberg formation (3.33–3.47 Ga), BGB, South Africa (Avice et al., 2017). The BARB 3 core (ICDP Project) mainly comprises a succession of white and black cherts and ultramafic rocks. All samples of this study consist of macro-crystalline quartz with different modes of emplacement in rocks from the BGB, probably linked to early hydrothermal activity (Hofmann and Harris, 2008). Trapped fluids contain Archaean paleo-atmospheric argon and xenon, and present Ar–Ar apparent ages showing excess $^{40}Ar^*$, with a tendency consistent with the age of the Kromberg formation (Avice et al., 2017).

All samples were neutron-irradiated to produce Ar proxy isotopes proportional to the Cl (^{38}Ar) and K (^{39}Ar) contents, and analyzed by in vacuo crushing and static mass spectrometry following methods and corrections given in Avice et al. (2017), Marty et al. (2013), and Pujol et al. (2011, 2013). North Pole samples were sequentially crushed under high vacuum with an activated piston (Pujol et al., 2011), whereas Barberton samples were sequentially crushed by squeezing the grains with a modified metal valve (Avice et al., 2017). Nitrogen and argon were also extracted by sequential crushing and combined nitrogen–argon measurements were carried out by static mass spectrometry following the method described in Humbert et al. (2000).

3. Results and discussion

With the conservative assumption that the partial pressure of ^{36}Ar did not vary significantly with time, we infer here that the seawater concentration of ^{36}Ar in the Archaean aeon was a function of temperature and salinity only (assuming a sea level location for atmospheric gas equilibrium). Thus, the $Cl/^{36}Ar$ and $K/^{36}Ar$ ratios of seawater would have varied primarily as a function of (i) these two parameters, and (ii) the Cl and K concentrations of the ancient seawater. Fig. 1 illustrates co-variations of these ratios for the analyzed samples, suggesting that the entire array of variations can be understood as mixing between several end-members, presumably different hydrothermal components, and a common end-member with a low salinity. The present-day salinity of the oceans is represented by a thick blue line for temperatures varying between 0 °C (a proxy of the average modern deep-sea temperature of 2 °C) and 75 °C (a plausible, but debated, temperature for the Archaean oceans; Robert and Chaussidon, 2006). At this scale of variations, data points for samples from two different localities (NW Australia and South Africa) are consistent with an ocean salinity comparable to, or lower than, the modern one, but not with a salinity being two times higher, or more, than the modern one. It is possible that some of the samples, e.g., BMG3-11, might have trapped freshwater and not seawater, in which case the correlations depicted in Fig. 1 would pass through the origin. However, such an origin is not supported by geochemical data (see sample description), which indicates the occurrence of a palaeo-seawater component in the FIs. Alternatively, some of the fluids released during stepwise extraction could have been contaminated by atmospheric noble gases other than those dissolved in trapped palaeoseawater. The effect of this contamination would be to add only ^{36}Ar to the extracted fluids, and therefore to have the correlations forced towards the origin in Fig. 1. This could be the case for some of the BMGA-3, and PI-06-03 stepwise data. Nevertheless, we think that these possibilities, namely, low salinity and/or atmospheric contamination, cannot account for several of the observed trends (e.g., those defined by the PI-02-39, BMG3-3, BMGA3-9 samples) that do not pass through the origin, but rather intersect the range of values expected for a seawater component (blue line in Fig. 1).

The $Cl/^{36}Ar$ and $K/^{36}Ar$ ratios could also have varied following other processes than component mixings. Evaporation in closed basins will tend to enrich Cl and K while maintaining ^{36}Ar at a constant level corresponding to the solubility equilibrium of water with the paleo-atmosphere. This could account for trends towards higher $Cl/^{36}Ar$ and $K/^{36}Ar$ ratios (Fig. 1), but not for the low ratios close to the origin. Likewise, boiling and phase separation in a hydrothermal environment will favour loss of gases including ^{36}Ar with respect to Cl and K, and could account for elevated $Cl/^{36}Ar$ and $K/^{36}Ar$ ratios, but not for the low end-member values. Hence the low $Cl/^{36}Ar$–$K/^{36}Ar$ end-member component of Fig. 1 is unlikely to be the result of secondary processing of trapped fluids.

Most samples in Fig. 1 show dispersion of data, suggesting that mixing between more than two hydrothermal components and/or secondary processing occurred. Each series of data for a given sample defines roughly variable Cl/K ratios (slopes of the correlations) that can be understood as chemically different hydrothermal end-member compositions. Thus, most of the slopes do not define the palaeoseawater composition. In hydrothermal systems, chlorine is mainly conservative upon temperature rise, mixing, and boiling, but the K concentration depends on temperature and rock lithology during water–rock interactions. K is indeed more mobile than Cl during hydrothermalism due to K^+ exchange with basalts authigenic mineral precipitation (e.g., Berner and Berner, 2012). In fact, the Cl/K ratios vary between 32.5 (PI-02-39-02) and 0.1 (PI-06-03), which is consistent with variable exchange of potassium between host rocks and hydrothermal waters.

Notably, The $Cl/^{36}Ar$ and $K/^{36}Ar$ ratios obtained for sample PI-02-39-2 yield a statistically good linear

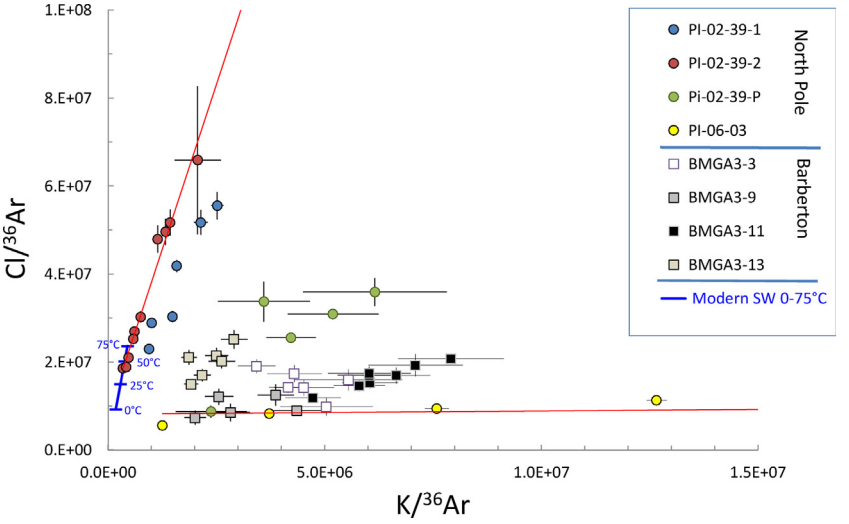

Fig. 1. $Cl/^{36}Ar$ vs $K/^{36}Ar$ variations for fluids trapped in Archaean quartz crystals from North Pole (NW Australia) and Barberton (South Africa) with ages between 3.0 and 3.5 Ga (data from Table 1). All samples host paleo-atmospheric argon and xenon and/or have Archaean Ar–Ar ages. Some of the data points are out of frame. The common symbol families represent stepwise crushing data for a given sample. Red lines represent linear correlations for samples PI-02-39-2 and PI-06-03, aimed at defining the upper and lower boundaries, respectively, for the observed Cl/K ratios. In this format, a two-component mixing results in a straight line joining the two end-members, whereas three-component mixing results in a cloud of data points embedded in a triangle limited by the component end-members. Data are consistent with mixings between different hydrothermal end-members rich in Cl and K, and a common end-member with low $Cl/^{36}Ar$ and $K/^{36}Ar$ ratios, regarded as the Archaean seawater component. The thick blue line represents the modern seawater salinity for temperatures between 0 and 75 °C.

regression (Figs. 1 and 2, MSWD = 0.75, probability of fit = 0.66). Chemical variations in this sample are, therefore, consistent with a two-component mixing between a seawater-like component and a hydrothermal component rich in Cl and K. The slope of the correlation is 32.5 ± 4.1 (2σ), comparable to the modern seawater ratio of 28.9. However, the slope is constrained by the value of the hydrothermal end-member, whereas the Cl/K ratio of the presumed Archaean seawater end-member appears closer to ~50, as suggested by data points with the lowest $Cl/^{36}Ar$ and $K/^{36}Ar$ ratios (Table 1, sample PI-02-39-2, Cl/K = 54.1 and 44.8 for crush 1 and crush 2 steps, respectively). This suggests that the Archaean seawater may be poorer in K relative to Cl than today. The hydrothermal end-member value (~31, Table 1) would then be coincidentally close to the modern Cl/K ratio, due to water-rock interactions (e.g., authigenic mineral precipitation) lowering the Archaean seawater ratio of ~50.

Using the equations given by Hamme and Emerson (2004), we have computed the evolution trends upon temperatures between 0 °C and 75 °C for three different seawater compositions having salinities 0.5, 1, and 2 times the modern salinity as represented by Cl and K (red, blue and green trends in Fig. 2). In this format, the intersection of the PI-02-39-02 correlation with these trends defines the composition and the temperature of the Archaean seawater end-member (Fig. 2). This intersect selects a salinity comparable to the modern one, and a seawater temperature in the range 20–40 °C. A warmer seawater in the Archaean than today is consistent with oxygen and silicon isotope variations in cherts and organic matter in the distant past (Robert and Chaussidon, 2006; Tartèse et al., 2017). Alternatively, such a noble gas-based temperature range may reflect the temperature of surface water in which atmospheric noble gases were dissolved, rather than the mean seawater temperature.

There is, however, an excess of radiogenic $^{40}Ar^*$ (labelled $^{40}Ar_{XS}$) in the initial fluid of the PI-02-39-02 sample. The $^{40}Ar/^{36}Ar$ ratio of the Archaean atmosphere around 3 Ga has been shown to be 143 ± 24 (1σ), but the initial ratio of the seawater component computed for this sample yields a higher, although imprecise, value of 1226 ± 920 (Fig. 3). $^{40}Ar_{XS}$ could have been contributed after deposition due to radiogenic ingrowth in the FIs but, given the K content of the trapped fluid, a negligible amount of $^{40}Ar_{XS}$ could have been contributed during the 3.5-Ga-long history of the quartz. Indeed, we compute that during 3.5 Ga, $1–3{\cdot}10^{-14}$ mol/g of radiogenic ^{40}Ar could have been generated by ^{40}K in FIs, corresponding to less than 1% of the total ^{40}Ar ($10^{-10}–10^{-11}$ mol/g). $^{40}Ar_{XS}$ could also have been injected from the host quartz, although the low K content of this phase might have not been sufficient to produce such an amount. $^{40}Ar_{XS}$ unsupported by other species, e.g., Cl, is common in fluid inclusions (e.g., Avice et al., 2017) and could result from water–rock interaction in an environment where the production of radiogenic ^{40}Ar from the decay of ^{40}K ($T_{1/2}$ = 1.25 Ga) was one order of magnitude higher than today. Contrary to ^{40}Ar, N_2 has been mostly conservative in Archaean fluid inclusions (Marty et al., 2013) and a correlation between $Cl/^{36}Ar$ vs. $N_2/^{36}Ar$ yields essentially the same information (Fig. 4), with a larger data dispersion. Here, the possible range of salinity values would be 0.5 to 1 times the modern one.

4. Implications

The present data are consistent with an Archaean seawater salinity comparable to, or even lower than, the

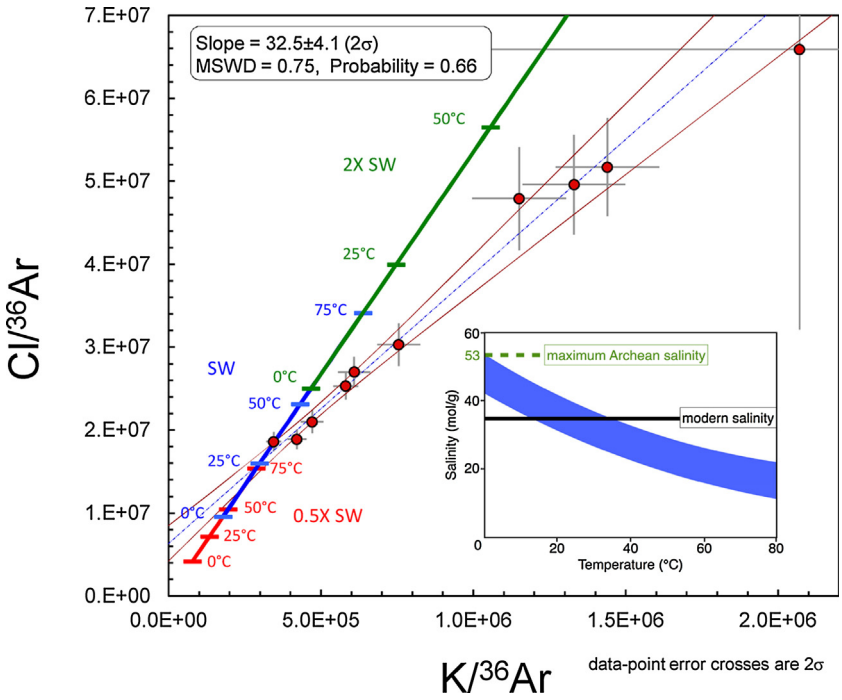

Fig. 2. PI-02-39-2 data correlation. For this sample, the good linear correlation is consistent with a two-component mixing. The red, blue and green thick lines represent salinities of 0.5×, 1×, and 2× the modern seawater composition, as expressed by Cl and K, for temperatures of 0, 25, 50, and 75 °C. These ranges represent the possible end-members between present-day ocean bottom temperatures of 2 °C and those proposed for Archaean oceans of up to 70 °C (Robert and Chaussidon, 2006). The insert shows the range of temperature-salinity which are consistent with the intersect of the data correlation with the lines defined above. The correlation is not consistent with salinities twice the modern value (de Ronde et al., 1997) or higher (Weiershauser and Spooner, 2005). For a modern-like salinity, a temperature in the range 20–40 °C is compatible with the data. For higher temperatures, the calculated salinity would be lower than the present-day one.

modern one. The relatively consistent salinity of the Earth's oceans since the Archaean has far reaching consequences regarding the volatile cycle and the emergence of life on the early Earth. Kendrick et al. (2017) proposed that up to 80% of the total budget of H_2O and heavy halogens now reside in surface reservoirs. Maintaining a constant salinity since the Archaean would require that the flux of H_2O and Cl to and from the oceans has also remained consistent since the Archaean. The dominant controls on early ocean salinity would be from the (i) variable rates of degassing and subduction recycling of H_2O and Cl and, (ii) the sequestering of Cl from the ocean into crustal evaporites and sediments. Continental freeboard studies have shown that the sea level change since the Archaean is limited to less than 500 m, indicating that the majority of the H_2O was degassed early and that the flux to the surface is roughly balanced by the return through subduction (Parai et al., 2012). In order to maintain a constant salinity since the Archaean, the flux of Cl to the surface is also required to be balanced by the return flux through subduction. Assuming that the majority of the Earth's volatiles were degassed early and that the oceans were almost fully formed during the Archaean, this would imply that H_2O and Cl are coupled during subduction recycling. Using current output fluxes of H_2O and Cl from MORB and OIB (Ito et al., 1983; Parai and Mukhopadhyay, 2012), it is estimated that the equivalent to 0.25–0.64 ocean masses of Cl and 0.15–0.53 ocean masses of H_2O have been subducted back to the mantle during the past 3.5 billion years.

The coupling of H_2O and Cl during subduction recycling is complicated by the potential for Cl to be sequestered into evaporite beds for geologically significant periods of time. Estimates of ocean salinity 1.2–2 times the modern values assumed that due to the presumed lower volumes of continental crust in the Archaean all evaporites and sedimentary brines were contained in the oceans (Holland, 1984; Knauth, 2005). As very little evidence remains for Archaean evaporites, this calculation relies on crustal evolution models to predict the timing of continental growth stabilization, estimated to be around 1.2 Ga (Knauth, 2005). However, recent crustal evolution models calculated using the crustal degassing of ^{36}Ar indicate that continental crust was formed much earlier, with the equivalent of 80% ± 10% of the current continental mass formed between 3.8 and 2.5 Ga (Dhuime et al., 2012; Pujol et al., 2013). The mass of the continental crust has therefore remained relatively stable since the Archaean. The drop in salinity towards modern values associated with the formation of continental evaporites and sedimentary brines may therefore have occurred earlier in the Earth's history.

The fluid inclusions data suggest that the Cl/K of the Archaean oceans (~50) could have been significantly higher than the modern value of 29. A major source of potassium in the oceans is now the erosion of the continental crust. The deficit of K in the Archaean oceans

Table 1
Argon, potassium and chlorine data for gases extracted by vacuum crushing of Archean hydrothermal quartz. See text for explanations on the analytical and data handling procedures.

Ech.		^{36}Ar mol/g	+/−	^{40}Ar/^{36}Ar	+/−	Cl mol/g	+/−	K mol/g	+/−	Cl/^{36}Ar	+/−	K/^{36}Ar	+/−	Cl/K	+/−	N_2 mol/g	+/−	N_2/^{36}Ar	+/−
PI02-39-1[a]	Crush 1	1.84E−14	3.80E−16	5092	195	4.17E−07	1.10E−08	b.d.l		2.30E+07	8.00E+05	9.50E+05	4.00E+04	24.2	1.3				
	Crush 2	1.68E−14	3.70E−16	6783	280	4.86E−07	1.30E−08	1.70E−08	5.00E−10	2.89E+07	1.00E+06	1.01E+06	3.72E+04	28.6	1.1				
	Crush 3	2.11E−14	4.00E−16	8971	306	8.83E−07	2.30E−08	3.35E−08	5.00E−10	4.18E+07	1.35E+06	1.59E+06	3.83E+04	26.4	0.8				
	Crush 4	7.95E−15	3.75E−16	10,242	844	4.11E−07	1.13E−08	1.70E−08	1.00E−09	5.17E+07	2.82E+06	2.14E+06	1.61E+05	24.2	1.6				
	Crush 5	7.58E−15	3.77E−16	11,053	954	4.21E−07	1.10E−08	1.91E−08	5.54E−10	5.56E+07	3.12E+06	2.52E+06	1.45E+05	22.0	0.9				
	Crush 6	1.18E−14	3.55E−16	5897	334	3.59E−07	1.10E−08	1.76E−08	5.35E−10	3.04E+07	1.30E+06	1.49E+06	6.35E+04	20.4	0.9				
PI02-39-2[a]	Crush 1	3.30E−14	5.30E−16	5585	143	6.15E−07	1.60E−08	1.14E−08	3.55E−10	1.86E+07	5.69E+05	3.45E+05	1.21E+04	53.9	2.2	1.28E−09	2.67E−11	3.88E+04	1.02E+03
	Crush 2	2.82E−14	4.66E−16	5466	155	5.33E−07	1.40E−08	1.19E−08	4.01E−10	1.89E+07	5.86E+05	4.21E+05	1.58E+04	44.8	1.9	9.83E−10	2.06E−11	3.48E+04	9.30E+02
	Crush 3	2.12E−14	4.07E−16	6111	216	4.46E−07	1.20E−08	1.00E−08	3.42E−10	2.10E+07	6.94E+05	4.71E+05	1.85E+04	44.6	1.9	6.57E−10	1.40E−11	3.09E+04	8.88E+02
	Crush 4	1.62E−14	3.79E−16	7716	341	4.38E−07	1.10E−08	9.90E−09	3.65E−10	2.70E+07	9.24E+05	6.09E+05	2.66E+04	44.2	2.0	6.75E−10	1.44E−11	4.16E+04	1.31E+03
	Crush 5	2.41E−14	4.36E−16	7093	226	6.10E−07	1.60E−08	1.40E−08	4.18E−10	2.53E+07	8.06E+05	5.81E+05	2.03E+04	43.6	1.7	9.64E−10	2.02E−11	4.00E+04	1.11E+03
	Crush 6	1.13E−14	3.73E−16	8330	514	3.41E−07	9.00E−09	8.50E−09	2.82E−10	3.03E+07	1.28E+06	7.55E+05	3.54E+04	40.1	1.7	5.66E−10	1.22E−11	5.03E+04	1.99E+03
	Crush 7	6.88E−15	4.04E−16	13,126	1298	3.30E−07	9.00E−09	7.90E−09	2.59E−10	4.79E+07	3.10E+06	1.15E+06	7.72E+04	41.8	1.8	6.20E−10	1.33E−11	9.01E+04	5.63E+03
	Crush 8	7.66E−15	3.93E−16	13,453	1199	3.96E−07	1.00E−08	1.10E−08	3.18E−10	5.17E+07	2.96E+06	1.44E+06	8.46E+04	36.0	1.4	5.12E−10	1.05E−10	6.69E+04	1.42E+04
	Crush 9	7.22E−15	3.99E−16	12,473	1178	3.58E−07	9.00E−09	9.60E−09	2.96E−10	4.96E+07	3.01E+06	1.33E+06	8.41E+04	37.3	1.5	5.43E−10	1.18E−11	7.52E+04	4.46E+03
	Crush 10	9.43E−16	5.94E−16	38,192	27,226	1.43E−07	4.00E−09	4.50E−09	1.71E−10	1.52E+08	9.56E+07	4.77E+06	3.01E+06	31.8	1.5	3.43E−10	7.82E−12	3.63E+05	2.29E+05
	Crush 11	2.08E−15	5.29E−16	15,773	5107	1.37E−07	4.00E−09	4.30E−09	1.67E−10	6.59E+07	1.69E+07	2.07E+06	5.32E+05	31.9	1.5	1.89E−10	4.99E−12	9.08E+04	2.32E+04
Pi-02-39-P[b]	Crush 1	4.6E−16	6.2E−17	9386	1270	1.5E−08	8.39E−11	1.64E−09	4.3E−10	3.38E+07	4.57E+06	3.60E+06	1.06E+06	9.4	2.5				
	Crush 2	6.1E−16	5.4E−17	11,993	1049	2.2E−08	1.453E−10	3.77E−09	9.6E−10	3.59E+07	3.15E+06	6.16E+06	1.66E+06	5.8	1.5				
	Crush 3	2.9E−16	4.4E−17	3392	518	2.5E−09	3.69E−11	6.80E−10	2.1E−10	8.74E+06	1.34E+06	2.38E+06	8.19E+05	3.7	1.1				
	Crush 4	1.0E−15	4.3E−17	8488	353	2.7E−08	1.428E−10	4.41E−09	5.7E−10	2.56E+07	1.07E+06	4.22E+06	5.73E+05	6.1	0.8				
	Crush 5	2.2E−15	8.1E−17	9913	368	6.8E−08	3.526E−10	1.14E−08	2.3E−09	3.09E+07	1.15E+06	5.19E+06	1.05E+06	6.0	1.2				
PI-06-3[c]	Crush 1	6.0E−14	5E−16	730	5	3.3E−07	1.2E−09	7.50E−08	1.00E−09	5.56E+06	5.08E+04	1.26E+06	1.98E+04	4.42	0.06				
	Crush 2	3.6E−14	3E−16	1058	10	3.0E−07	1.4E−09	1.35E−07	3.00E−09	8.30E+06	7.87E+04	3.72E+06	8.82E+04	2.23	0.05				
	Crush 3	1.4E−14	5E−16	1115	38	1.3E−07	1.1E−09	1.07E−07	1.00E−09	9.42E+06	3.43E+05	7.59E+06	2.78E+05	1.24	0.02				
	Crush 4	3.0E−14	5E−16	1433	21	3.4E−07	2.3E−09	3.81E−07	3.00E−09	1.13E+07	2.02E+05	1.27E+07	2.33E+05	0.89	0.01				
	Crush 5	1.1E−14	5E−16	3504	166	1.4E−07	1.3E−09	5.64E−07	3.00E−09	1.25E+07	5.80E+05	5.13E+07	2.35E+06	0.24	0.00				
	Crush 6	9.6E−15	3E−16	5410	178	1.3E−07	1.2E−09	8.60E−07	3.00E−09	1.38E+07	4.50E+05	8.96E+07	2.82E+06	0.15	0.00				
Barberton[d]																			
BMGA3-13	Crush 1	8.0E−14	4.4E−15	3611	57	1.35E−06	7.57E−08	1.73E−07	1.22E−08	1.70E+07	1.34E+06	2.17E+06	1.96E+05	7.8	0.9				
	Crush 2	3.7E−14	2.1E−15	4376	90	7.83E−07	4.39E−08	6.95E−08	5.21E−09	2.11E+07	1.69E+06	1.87E+06	1.76E+05	11.3	1.4				
	Crush 3	1.5E−14	8.8E−16	3607	83	3.23E−07	1.83E−08	3.77E−08	3.40E−09	2.15E+07	1.74E+06	2.50E+06	2.69E+05	8.6	1.2				
	Crush 4	1.1E−14	6.7E−16	3980	111	2.78E−07	1.55E−08	3.21E−08	2.80E−09	2.52E+07	2.07E+06	2.91E+06	3.09E+05	8.7	1.2				
	Crush 5	1.3E−14	7.3E−16	3294	72	2.56E−07	1.43E−08	3.32E−08	3.41E−09	2.02E+07	1.62E+06	2.62E+06	3.09E+05	7.7	1.1				
	Crush 6	2.8E−14	1.6E−15	2388	33	4.24E−07	2.37E−08	5.43E−08	3.54E−09	1.50E+07	1.18E+06	1.92E+06	1.64E+05	7.8	0.9				

Table 1 (*Continued*)

Ech.		^{36}Ar mol/g	+/−	^{40}Ar/^{36}Ar	+/−	Cl mol/g	+/−	K mol/g	+/−	Cl/^{36}Ar	+/−	K/^{36}Ar	+/−	Cl/K	+/−	N_2 mol/g	+/−	N_2/^{36}Ar	+/−
BMGA3-11	Crush 1	9.77E−16		5.69E−17	9606	763	1.16E−08	6.78E−10	4.62E−09	5.66E−10	1.19E+07	9.79E+05	4.73E+06	6.42E+05	2.5	0.4				
	Crush 2	3.01E−15		1.94E−16	12,491	1049	4.41E−08	2.49E−09	1.75E−08	1.39E−09	1.46E+07	1.25E+06	5.80E+06	5.93E+05	2.5	0.3				
	Crush 3	4.18E−15		2.45E−16	12662	1011	6.39E−08	3.73E−09	2.53E−08	2.26E−09	1.53E+07	1.27E+06	6.05E+06	6.47E+05	2.5	0.3				
	Crush 4	1.24E−15		1.46E−16	16272	2113	2.39E−08	1.41E−09	8.77E−09	8.60E−10	1.93E+07	2.55E+06	7.10E+06	1.09E+06	2.7	0.6				
	Crush 5	4.49E−16		4.03E−17	13726	1439	7.62E−09	4.46E−10	2.99E−09	2.24E−10	1.70E+07	1.82E+06	6.65E+06	7.78E+05	2.5	0.4				
	Crush 6	4.02E−16		2.35E−17	11834	943	4.46E−09	2.78E−10	0.00E+00	1.57E−10	1.11E+07	9.48E+05								
	Crush 7	7.25E−16		4.42E−17	14101	1150	1.23E−08	7.11E−10	4.37E−09	4.64E−10	1.70E+07	1.43E+06	6.03E+06	7.39E+05	2.8	0.4				
	Crush 8	1.40E−15		9.09E−17	14176	1200	2.43E−08	1.57E−09	8.43E−09	1.22E−09	1.74E+07	1.60E+06	6.03E+06	9.57E+05	2.9	0.5				
	Crush 9	5.74E−16		6.45E−17	18,893	2357	1.19E−08	7.08E−10	4.54E−09	4.79E−10	2.07E+07	2.64E+06	7.91E+06	1.22E+06	2.6	0.5				
BMGA3-9	Crush 1	2.05E−15		1.30E−15	5809	479	1.75E−07	1.03E−08	b.d.l		8.54E+06	7.30E+05	n.d.							
	Crush 2	4.43E−14		2.50E−15	3207	250	2.39E−07	1.37E−08	b.d.l		5.39E+06	4.30E+05	n.d.							
	Crush 3	5.02E−14		2.80E−15	4050	314	3.69E−07	2.14E−08	1.01E−07	1.10E−08	7.35E+06	5.90E+05	2.01E+06	2.50E+05	3.7	0.5				
	Crush 4	4.40E−15	7E−16		5479	875	3.93E−08	2.37E−09	1.91E−08	1.11E−09	8.95E+06	1.45E+06	4.36E+06	7.00E+05	2.1	0.5				
	Crush 5	1.74E−14		1.30E−15	5142	470	1.49E−07	8.55E−09	4.94E−08	6.82E−09	8.56E+06	8.00E+05	2.83E+06	4.40E+05	3.0	0.5				
	Crush 6	1.31E−14		8.00E−16	7077	571	1.59E−07	9.33E−09	3.34E−08	3.83E−09	1.22E+07	1.02E+06	2.56E+06	3.30E+05	4.7	0.7				
	Crush 7	8.10E−15		5.00E−16	6409	520	1.02E−07	5.81E−09	3.15E−08	2.88E−09	1.25E+07	1.04E+06	3.87E+06	4.20E+05	3.2	0.4				
BMGA3-3	Crush 1	6.50E−15		4.00E−16	6179	513	1.24E−07	6.97E−09	2.23E−08	2.39E−09	1.91E+07	1.61E+06	3.43E+06	4.30E+05	5.6	0.8				
	Crush 2	7.60E−15		5.00E−16	7326	605	1.08E−07	6.08E−09	3.16E−08	2.81E−09	1.43E+07	1.20E+06	4.16E+06	4.50E+05	3.4	0.5				
	Crush 3	3.00E−15		5.00E−16	5657	1041	2.98E−08	2.89E−09	1.53E−08	1.82E−09	9.83E+06	1.97E+06	5.04E+06	1.07E+06	2.0	0.6				
	Crush 4	7.00E−15		8.00E−16	7131	914	9.99E−08	5.96E−09	3.18E−08	3.20E−09	1.42E+07	1.85E+06	4.52E+06	6.90E+05	3.1	0.6				
	Crush 5	3.20E−15		4.00E−16	7173	1074	5.07E−08	2.94E−09	1.76E−08	3.09E−09	1.60E+07	2.42E+06	5.55E+06	1.24E+06	2.9	0.8				
	Crush 6	6.80E−15		7.00E−16	8558	943	1.19E−07	6.66E−09	2.94E−08	3.29E−09	1.74E+07	1.93E+06	4.30E+06	6.30E+05	4.0	0.7				

[a] Marty et al., 2013.
[b] Pujol et al., 2013.
[c] Pujol et al., 2011.
[d] Avice et al., 2017 and unpublished.
b.d.l: below detection limit; n.d.: not determined.

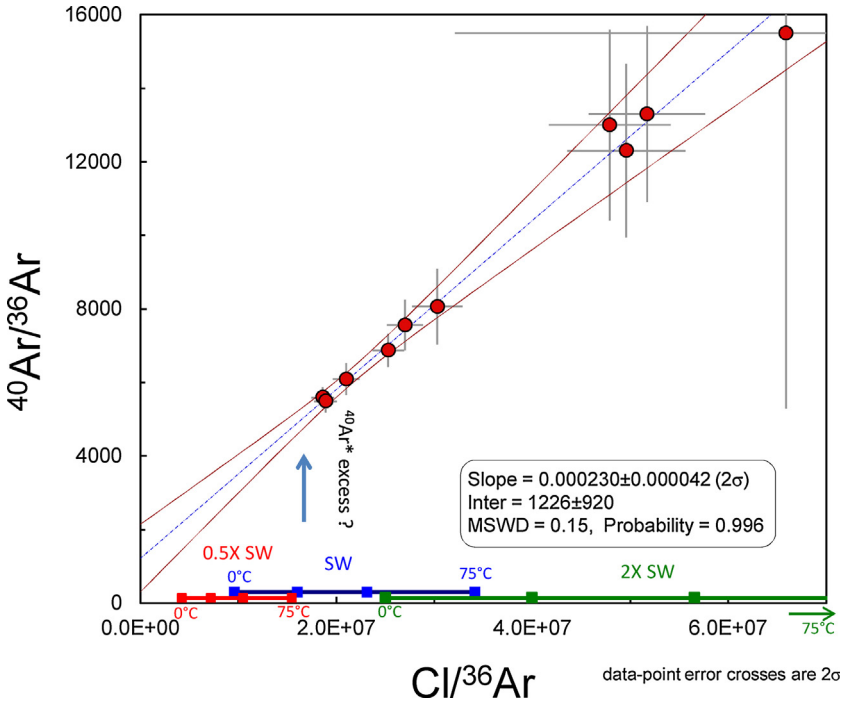

Fig. 3. PI-02-39-2 data. In this $^{40}Ar/^{36}Ar$ vs. $Cl/^{36}Ar$ format, a fair correlation is also observed, consistent with mixing between a low-salinity end-member and an evolved fluid component rich in radiogenic ^{40}Ar and in Cl. The correlation defines a low $^{40}Ar/^{36}Ar$–$Cl/^{36}Ar$ end-member, presumably representing the seawater component, and a high $^{40}Ar/^{36}Ar$–$Cl/^{36}Ar$ end-member, representing the hydrothermal component. Note that the low $^{40}Ar/^{36}Ar$ component has radiogenic $^{40}Ar^*$ in excess relative to the atmospheric composition, and could represent a moderately evolved seawater component having incorporated $^{40}Ar^*$, but not Cl, from country rocks. The red, blue, and green thick lines represent salinities of 0.5×, 1× and 2× the modern seawater one, as expressed by Cl and K, for temperatures of 0, 25, 50 and 75 °C (modern seawater symbols have been offset for clarity).

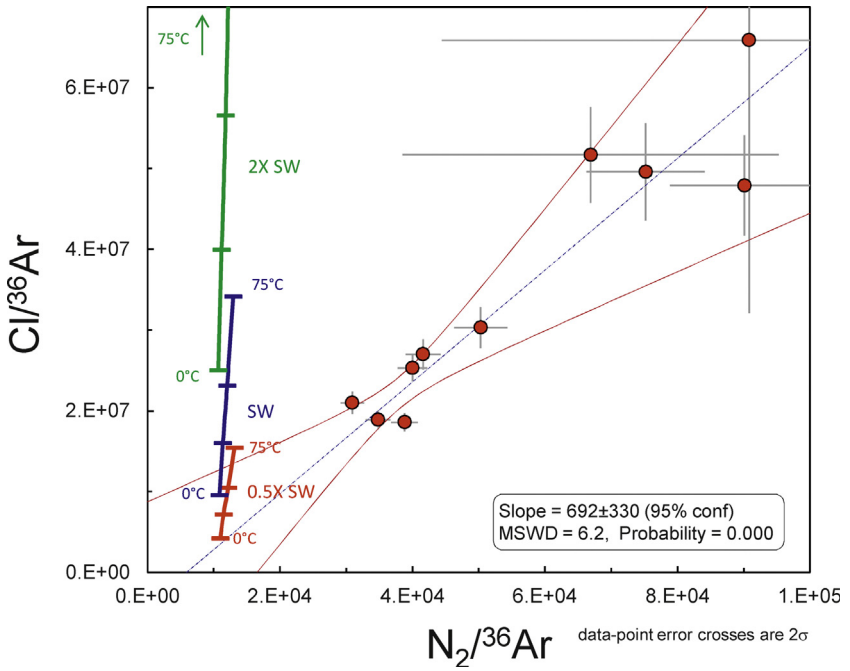

Fig. 4. $Cl/^{36}Ar$ vs. $N_2/^{36}Ar$ data for sample PI-02-39-2. Same symbols as in Fig. 3.

could therefore be related to the smaller continental reservoir 3.5 Ga ago. However, the cycle of oceanic potassium is poorly known, in particular the K flux between the oceans and the oceanic crust and the uptake of K by sediments (see Berner and Berner, 2012).

The properties of the Archaean oceans such as salinity, temperature and chemistry all played a crucial role in the emergence of life. Salinity levels greater than modern seawater are suggested to have suppressed the evolution of macroscopic marine life in the Archaean (Knauth, 1998). The development of macroscopic life might have been limited, as metazoan life forms cannot tolerate high-salinity conditions (Hay et al., 2006). This is consistent with cyanobacteria (relatively salt tolerant) dominating the Precambrian fossil record (Knauth, 2005). Our data are however consistent with Archaean oceans' salinity being comparable to that of the modern oceans at a plausible temperature range of 0–75 °C.

This implies that the early forms of Archaean life were not necessarily salt tolerant or restricted to the more dilute waters of estuaries (Knauth, 1998), but might have already been widespread throughout the oceans. The limited diversity of the eukaryotes within the Proterozoic fossil record (Schopf and Klein, 1992) may therefore be accounted for by nutrient limitation and/or widespread sulfidic conditions in the early oceans (Anbar and Knoll, 2002). Likewise, the lack of evidence for Proterozoic metazoans in the fossil record could indicate that early metazoans developed in environments with low preservation potentials, such as the Archaean deep-sea environments, which are erased at subduction zones. Note that a constant global ocean salinity through time does not exclude the possibility that saltier environments existed during the Archaean, as evidenced by highly saline early seawater trapped in fluid inclusions within 3.2-Ga quartz crystals (de Ronde et al., 1997). In fact, the presence of evaporites on the Archaean crust and evidence of saltier environments hint at potential for localized evaporation and formation of habitats such as lagoons suitable for life (Park, 1977). Our data also support the possibility that significant amounts of oxygen were already dissolved in the oceans during the Archaean, as oxygen solubility in seawater increases with decreasing salinity and temperature (Weiss, 1970).

5. Conclusion

Data for FIs in Archaean quartz samples from different localities present chemical variations which are consistent with mixings between several hydrothermal end-members and a common component regarded as Archaean seawater. The latter appears to have a salinity (Cl) comparable to that of modern seawater. We conclude that the present data appear to exclude a salinity twice higher than the modern value (Figs. 1 and 2). The Cl/K ratio of Archaean seawater (~50) could have been lower than the present-day one (29), suggesting that the Archaean oceans contained less potassium than the modern oceans.

The budget of Cl and K in the oceans is still largely undocumented. Rivers are the main input flux of chlorine to the oceans ($2.1 \cdot 10^{14}$ g/yr), and evaporite precipitation can be a significant output flux, provided that evaporites are stabilized onto continents (Berner and Berner, 2012). Overall, the oceanic chloride budget appears to be in a steady state on the long term, at least since 600 Ma (Berner and Berner, 2012). Major unknowns are the fluxes at mid-ocean ridges, which could be significant in either way (Edmond et al., 1979). These uncertainties leave room for the case of a salinity (e.g., Cl) of the Archaean oceans comparable to the modern one. The oceanic cycle of potassium is even less documented. The low potassium content of the Archaean oceans suggested by this study could be related to a smaller volume of Archaean felsic crust than at Present. Indeed, a major source of potassium in the oceans is now the erosion of the continental crust, thus the deficit of K in the Archaean oceans may be the result of reduced runoff from smaller continental reservoirs.

Acknowledgments

This study was funded by the European Research Council (FP/7 2007–2013, grant agreement 267255). Ray Burgess is thanked for mentorship and assistance during Ar–Ar experiments. Samples were made available through collaborations with Pascal Philippot, Axel Hofmann, and Nick Arndt. We are grateful to Mark Kendricks and Romain Tartèse for detailed and constructive comments, and to Marc Chaussidon for edition and suggestions. This is CRPG contribution # 2558.

References

Anbar, A.D., Knoll, A., 2002. Proterozoic ocean chemistry and evolution: a bioinorganic bridge? Science 297, 1137–1142.
Avice, G., Marty, B., Burgess, R., 2017. The origin and degassing history of the Earth's atmosphere revealed by Archean xenon. Nat. Commun. 8, 15455.
Berner, E.K., Berner, R.A., 2012. Global Environment, 2nd ed. Princeton University Press, Princeton & Oxford.
Coltice, N., Marty, B., Yokochi, R., 2009. Xenon isotope constraints on the thermal evolution of the early Earth. Chem. Geol. 266, 4–9.
de Ronde, C.E.J., Channer, D.M. deR., Faure, K., Bray, C.J., Spooner, E.T.C., 1997. Fluid chemistry of Archean seafloor hydrothermal vents: Implications for the composition of circa 3.2 Ga seawater. Geochim. Cosmochim. Acta 61, 4025–4042.
Dhuime, B., Hawkesworth, C.J., Cawood, P.A., Storey, C.D., 2012. A change in the geodynamics of continental growth 3 billion years ago. Science 335, 1334–1336.
Edmond, J.M., Measures, C., McDuff, R.E., Chan, L.H., Collier, R., Grant, B., Gordon, L.I., Corliss, J.B., 1979. Ridge crest hydrothermal activity and the balances of the major and minor elements in the ocean: the Galapagos data. Earth Planet. Sci. Lett. 46, 1–18.
Foriel, J., Philippot, P., Rey, P., Somogyi, A., Banks, D., Menez, B., 2004. Biological control of Cl/Br and low sulfate concentration in a 3.5-Gyr-old seawater from North Pole, Western Australia. Earth Planet. Sci. Lett. 228, 451–463.
Hamme, R.C., Emerson, S.R., 2004. The solubility of neon, nitrogen and argon in distilled water and seawater. Deep. Res. Part I Oceanogr. Res. Pap. 51, 1517–1528.
Hay, W.W., Migdisov, A., Balukhovsky, A.N., Wold, C.N., Flögel, S., Söding, E., 2006. Evaporites and the salinity of the ocean during the Phanerozoic: implications for climate, ocean circulation and life. Palaeogeogr. Palaeoclimatol. Palaeoecol. 240, 3–46.
Hofmann, A., Harris, C., 2008. Silica alteration zones in the Barberton greenstone belt: A window into subseafloor processes 3.5–3.3 Ga ago. Chem. Geol. 257, 224–242.
Holland, H.D., 1984. The Chemical Evolution of the Atmosphere and Oceans. Princeton University Press, Princeton.

Humbert, F., Libourel, G., France-Lanord, C., Zimmermann, L., Marty, B., 2000. CO_2-laser extraction-static mass spectrometry analysis on ultra-low concentrations of nitrogen in silicates. Geostand. Newslett. 24, 255–260.

Ito, E., Harris, D.M., Anderson, A.T., 1983. Alteration of oceanic crust and geologic cycling of chlorine and water. Geochim. Cosmochim. Acta 47, 1613–1624.

Kendrick, M.A., 2012. High precision Cl, Br and I determinations in mineral standards using the noble gas method. Chem. Geol. 292, 116–126.

Kendrick, M.A., Burgess, R., Pattrick, R.A.D., Turner, P.G., 2001. Halogen and Ar–Ar age determinations of inclusions within quartz veins from porphyry copper deposits using complementary noble gas extraction techniques. Chem. Geol. 177, 351–370.

Kendrick, M.A., Kamenetsky, V.S., Phillips, D., Honda, M., 2012. Halogen systematics (Cl, Br, I) in Mid-Ocean Ridge Basalts: A Macquarie Island case study. Geochim. Cosmochim. Acta 81, 82–93.

Kendrick, M., Hémond, C., Kamenetsky, V., Danyushevsky, L., Devey, C.W., Rodemann, T., Perfit, M., 2017. Seawater cycled throughout Earth's mantle in partially serpentinized lithosphere. Nat. Geosci. 10, 222–228.

Knauth, L.P., 1998. Salinity history of the Earth's early ocean. Nature 395, 554–555.

Knauth, L.P., 2005. Temperature and salinity history of the Precambrian ocean: Implications for the course of microbial evolution. Palaeogeogr. Palaeoclimatol. Palaeoecol. 219, 53–69.

Lichtenegger, H.I.M., Lammer, H., Griessmeier, J.M., Kulikov, Y.N., von Paris, P., Hausleitner, W., Krauss, S., Rauer, H., 2010. Aeronomical evidence for higher CO_2 levels during Earth's Hadean epoch. Icarus 210, 1–7.

Lowe, D.R., Byerly, G.R., 2003. Ironstone pods in the Archean Barberton greenstone belt, South Africa: Earth's oldest seafloor hydrothermal vents reinterpreted as Quaternary subaerial springs. Geology 31, 909–912.

Marty, B., Zimmermann, L., Pujol, M., Burgess, R., Philippot, P., 2013. Nitrogen isotopic composition and density of the Archean atmosphere. Science 342, 101–104.

Ozima, M., Podosek, F.A., 2002. Noble Gas Gochemistry. Cambridge University Press, Cambridge.

Parai, R., Mukhopadhyay, S., 2012. How large is the subducted water flux? New constraints on mantle regassing rates. Earth Planet. Sci. Lett. 317, 396–406.

Park, R.K., 1977. The preservation potential of some recent stromatolites. Sedimentology 24, 485–506.

Pujol, M., Marty, B., Burgess, R., 2011. Chondritic-like xenon trapped in Archean rocks: a possible signature of the ancient atmosphere. Earth Planet. Sci. Lett. 308, 298–306.

Pujol, M., Marty, B., Burgess, R., Turner, G., Philippot, P., 2013. Argon isotopic composition of Archean atmosphere probes early Earth geodynamics. Nature 498, 87–90.

Robert, F., Chaussidon, M., 2006. A palaeotemperature curve for the Precambrian oceans based on silicon isotopes in cherts. Nature 443, 969–972.

Schopf, J.W., Klein, C., 1992. The Proterozoic Biosphere: A Multidisciplinary Study. Cambridge University Press.

Tartèse, R., Chaussidon, M., Gurenko, A., Delarue, F., Robert, F., 2017. Warm Archaean oceans reconstructed from oxygen isotope composition of early-life remnants. Geochem. Perspect. Lett. 55–65.

Weiershauser, L., Spooner, E.T.C., 2005. Seafloor hydrothermal fluids, Ben Nevis area, Abitibi Greenstone Belt: Implications for Archean (~2.7 Ga) seawater properties. Precambrian Res. 138, 89–123.

Weiss, R., 1970. The solubility of nitrogen, oxygen and argon in water and seawater. Deep Sea Res. 17, 721–735.